



Observations of the Effects of a Clay Layer on Suction Bucket Installation in Sand

Raffaele Ragni¹; Britta Bienen, Aff.M.ASCE²; Conleth D. O'Loughlin³,
Samuel A. Stanier⁴; Mark J. Cassidy⁵; and Neil Morgan⁶

Abstract: Suction buckets are becoming established as a viable foundation solution for offshore wind turbines. In sand, suction-induced seepage flow reduces effective stresses at the skirt tips, which decreases penetration resistance. However, layered seabeds are often encountered in areas of offshore wind farm development. The effect of the presence of a clay layer on the suction-induced seepage flow in the sand layer is not well understood. Therefore in this study, the effects of a clay layer on suction bucket installation in dense sand was investigated. This was achieved by analyzing images of a half-bucket installed against a Perspex window. The images were captured during tests performed in a geotechnical centrifuge, such that the stress levels are realistic and relevant to field conditions. Installations in sand-over-clay were unproblematic and characterized by deformation of the sand-clay interface, with no clear interruption of the seepage flow. Installations in clay-over-sand were also successful. Uplift of the clay plug was identified as the mechanism to transfer suction to the underlying sand, creating seepage flow and thus facilitating further skirt penetration rather than terminating the installation. DOI: [10.1061/\(ASCE\)GT.1943-5606.0002217](https://doi.org/10.1061/(ASCE)GT.1943-5606.0002217). © 2020 American Society of Civil Engineers.

Introduction

Suction buckets are increasingly considered as foundation solutions for offshore wind turbines (OWT) (e.g., in the North Sea at the

¹Geotechnical Engineer, Norwegian Geotechnical Institute, Level 7/40 St Georges Terrace, Perth, WA 6000, Australia; formerly, Research Associate, Centre for Offshore Foundation Systems, Lloyd's Register Centre of Excellence for Offshore Foundations, Univ. of Western Australia, 35 Stirling Hwy., Crawley, Perth, WA 6009 Australia. Email: raffaele.ragni@ngi.no

²Associate Professor and Lloyd's Register Foundation Chair, Centre for Offshore Foundation Systems, Lloyd's Register Centre of Excellence for Offshore Foundations, Univ. of Western Australia, 35 Stirling Hwy., Crawley, Perth, WA 6009 Australia (corresponding author). ORCID: <https://orcid.org/0000-0002-0342-0698>. Email: britta.bienen@uwa.edu.au

³Associate Professor, Centre for Offshore Foundation Systems, Lloyd's Register Centre of Excellence for Offshore Foundations, Univ. of Western Australia, 35 Stirling Hwy., Crawley, Perth, WA 6009 Australia. ORCID: <https://orcid.org/0000-0002-5823-6265>. Email: conleth.oloughlin@uwa.edu.au

⁴University Senior Lecturer, Dept. of Engineering, Cambridge Univ., Trumpington St., Cambridge CB2 1PZ, UK; formerly, Senior Research Fellow, Centre for Offshore Foundation Systems, Lloyd's Register Centre of Excellence for Offshore Foundations, Univ. of Western Australia, 35 Stirling Hwy., Crawley, Perth, WA 6009 Australia. Email: sas229@cam.ac.uk

⁵Professor, Melbourne School of Engineering, Univ. of Melbourne, Old Engineering Bldg., Parkville, VIC 3010, Australia; formerly, Professor and Director, Centre for Offshore Foundation Systems, Lloyd's Register Centre of Excellence for Offshore Foundations, Univ. of Western Australia, 35 Stirling Hwy., Crawley, Perth, WA 6009 Australia. Email: mark.cassidy@unimelb.edu.au

⁶Principal Geotechnical Engineer, Lloyd's Register EMEA, Kingswells Causeway, Prime Four Business Park, Kingswells, Aberdeen AB15 8PU, UK. Email: neil.morgan@lr.org

Note. This manuscript was submitted on April 23, 2019; approved on October 23, 2019; published online on March 9, 2020. Discussion period open until August 9, 2020; separate discussions must be submitted for individual papers. This paper is part of the *Journal of Geotechnical and Geoenvironmental Engineering*, © ASCE, ISSN 1090-0241.

Borkum Riffgrund 1/2 and Aberdeen Bay sites). Advantages include fast installation [in Aberdeen Bay the installation of the last jacket with ~10-m-diameter suction buckets took 2 h and 40 min (Offshorewind.biz 2018), compared to commonly used monopiles, which take a day or more to install (Lacal-Arántegui et al. 2018) that is practically silent, which minimizes disturbance to marine fauna.

The concept involves a steel cylinder that is open-ended at the bottom and closed at the top. Initial penetration is achieved through self-weight, which creates a pathway for seepage flow through the soil around the embedded skirt tips. Water is then pumped from the bucket interior, resulting in a differential pressure (referred to as suction) across the bucket lid. For installations in clay, suction creates a downward force, which drives the bucket further into the seabed (Houlsby and Byrne 2005a). In sand, the seepage flow induced by suction—resulting from the relatively high soil permeability—reduces the effective stress below the skirt tips, facilitating installation (Erbrich and Tjelta 1999; Houlsby and Byrne 2005b; Andersen et al. 2008; Senders and Randolph 2009).

Although sandy soils prevail in the shallow waters where offshore wind farms have so far developed, exposure to geological events often causes soil layering, with significant variation of the soil properties both vertically and horizontally (Dove et al. 2016; Cotterill et al. 2017; Sturm 2017). Andersen et al. (2008) noted that the interbedded layers of clay in sand may prevent seepage flow, and hinder the reduction in effective stresses needed for penetration.

Where clay is overlain by sand, suction bucket installation may broadly follow the schematic in Fig. 1(a). Seepage flow develops when a suction p_1 is applied, provided the skirt tips remain in the sand layer. As the skirts approach and penetrate the low permeability clay, seepage flow may be restricted, which would affect the seepage flow and reduction in effective stresses at the skirt tips (Andersen et al. 2008; Zhu 2018).

Where sand is overlain by clay [Fig. 1(b)], sufficient suction p_1 will cause shearing at the skirt-clay interface, facilitating bucket penetration through the clay. However, the clay layer will initially prevent any seepage flow from developing in the underlying sand. Hence, no reduction in effective stresses below the skirt tips is

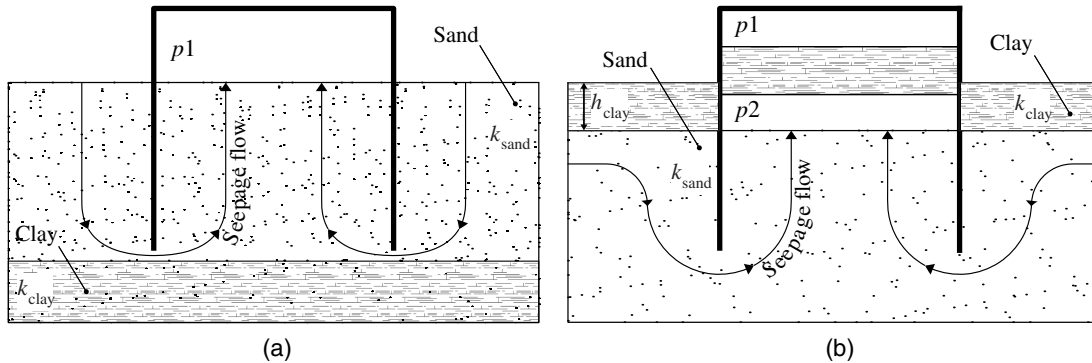


Fig. 1. Schematic representation of suction bucket installation in (a) permeable soil with underlying impermeable layer; and (b) in permeable soil overlain by an impermeable layer.

experienced as the bucket advances through the underlying sand, which may hinder installation when high penetration resistance is encountered. However, if the applied suction p_1 is sufficient to fail the clay plug (i.e., $p_1 \geq p_{\text{plug}}$), clay uplift is expected to occur, such that a suction pressure $p_2 = p_1 - p_{\text{plug}}$ will form in the newly formed gap, which in turn will generate seepage flow (Senders et al. 2007). Reduced-scale model tests both in a centrifuge (Tran et al. 2007; Watson et al. 2006; and Senders et al. 2007) and at single gravity (Cotter 2009) show that installation in sand overlain by a less permeable material is possible. However, the governing mechanisms are not as well understood, such that extrapolation of this performance to seabed profiles beyond the current limits of experience will introduce uncertainty, as discussed for recent case studies (Panayides et al. 2017; Sauve et al. 2017). Furthermore, suction installation may alter the soil state within or surrounding the bucket, and such changes may affect in-service performance.

This paper therefore considers the performance of suction buckets in layered seabeds through an experimental study that visualizes the effects of a clay layer on suction bucket installation in dense sand, where effective stress reduction through seepage flow around the skirt tip is essential for successful installation. The study aims to:

1. Reveal the deformation mechanism and changes in soil state governing suction bucket installation in sand-over-clay and clay-over-sand profiles;
2. Assess the effects of pumping flow rate and thickness of the clay layer on installations in clay-over-sand profiles; and
3. Assess the potential for—and the consequences of—any clay plug uplift.

To address these aims, particle image velocimetry (PIV) analyses (Stanier and White 2013; Stanier et al. 2016) were carried out on images of suction bucket installations in a geotechnical

centrifuge. The paper represents the first observation of the effects of a clay layer on suction bucket installation in sand, at relevant stress levels.

Experimental Details

The experiments were conducted using a half-model suction bucket installed using a combination of self-weight and suction assistance adjacent to a window, allowing photography of the bucket interior during installation. The techniques and approach used in the experiments are reported in detail in Ragni et al. (2019), and described in brief in the following sections.

The experimental program involved eight suction bucket installations, two in sand-over-clay (SoC) and six in clay-over-sand (CoS), with the focus placed on the latter as this was considered to have higher potential to be problematic. Jacked installations were also conducted for each soil profile type to provide a basis for assessing the effect of suction installation. Installations in clay-over-sand investigated the role of clay thickness and pumping rate. Table 1 provides a summary of all tests performed and the main characteristics of the soil samples.

Centrifuge and Experimental Apparatus

The experiments were performed at 100g in the 1.8-m-radius beam centrifuge at the National Geotechnical Centrifuge Facility located at The University of Western Australia (Randolph et al. 1991; Randolph and Gaudin 2017).

Fig. 2(a) shows an overview of the centrifuge setup. A centrifuge sample container (strongbox) housed a smaller PIV sample box (with inner dimensions of 335 × 225 × 300 mm), which had

Table 1. Summary of experimental program

Test	Top layer	Top layer thickness target actual (h/L)	Relative density of sand, D_r (%)	Undrained shear strength of clay ^a , s_u (kPa)	Pumping flow rate, q_{pump} (mm^3/s)
SoC_1	Sand	0.6 0.62	100	~30	N/A (Jacked)
SoC_2	Sand	0.6 0.59	100	~30	235.6 (Med)
CoS_1	Clay	0.2 0.2	99	~12.8	N/A (Jacked)
CoS_2	Clay	0.2 0.19	91	~12.8	117.8 (Low)
CoS_3	Clay	0.2 0.19	91	~12.8	235.6 (Med)
CoS_4	Clay	0.2 0.17	94	~12.8	1,178.1 (High)
CoS_5	Clay	0.4 0.36	87	~14.8	235.6 (Med)
CoS_6	Clay	0.6 0.56	100	~16.2	235.6 (Med)

^aEstimated according to Ladd et al. (1977).

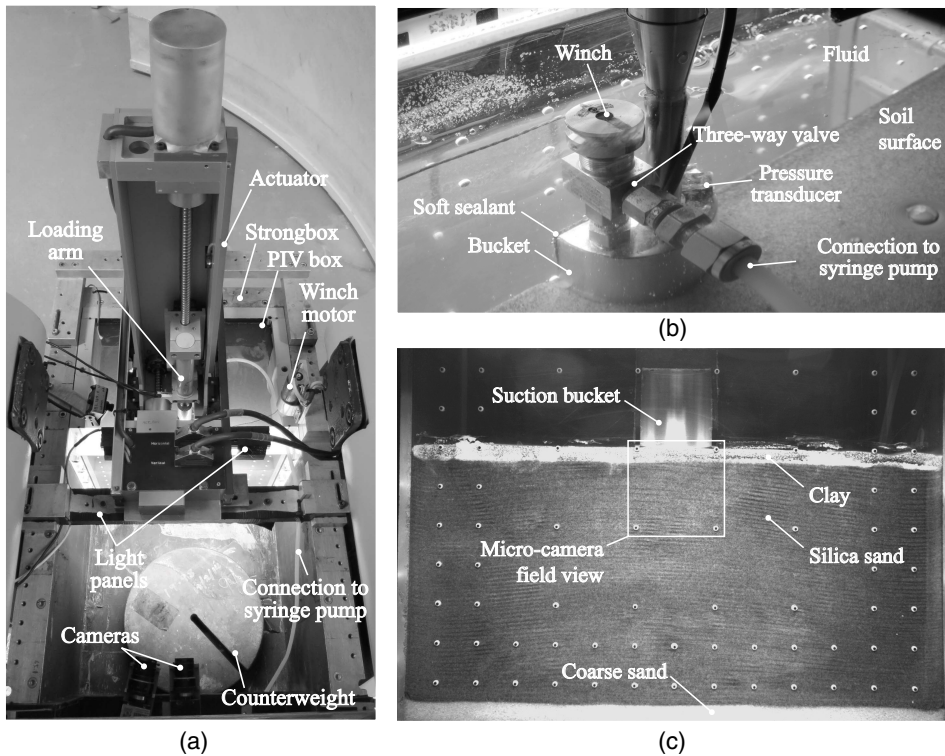


Fig. 2. Centrifuge experimental apparatus: (a) overview; (b) half-model bucket at PIV window; and (c) macro camera view (with micro camera field of view shown).

a 50-mm-thick transparent acrylic window, sufficient to avoid excessive deflection (Haigh and Madabhushi 2014). The half-model bucket was fabricated from a solid block of aluminum and was anodized. It had a diameter $D = 50$ mm and skirt length $L = 50$ mm, i.e., a geometrical aspect ratio $L/D = 1$, which is within the range of relevant geometries for shallow water applications (e.g., Borkum Riffgrund 1 and 2, Aberdeen Bay Offshore Wind Farm). The seal between the suction bucket model and the PIV transparent window was obtained with a combination of soft sealant close-cell foam tape on the majority of the interface, and hard rubber at the bucket tips (Ragni et al. 2019). The interface was lubricated prior to each test with petroleum jelly to minimize friction. The penetration resistance and applied suction place significant stresses on the sealant material and the skirt-seal interface. The skirt thickness was $t = 2$ mm (i.e., $D/t = 25$), as this was the minimum required to maintain the seal (along the skirt, between skirt and acrylic window) during installation (Ragni et al. 2019). Although lower than typical D/t values, which may be closer to 200, Tran and Randolph (2008) demonstrated that the skirt thickness has only a marginal effect on the suction required during installation.

The model bucket was penetrated adjacent to the window of the PIV sample box using the vertical axis of an electromechanical actuator under displacement control (modeling the self-weight installation stage) before holding the load acting at the end of the self-weight installation stage and using a syringe pump to extract fluid from the bucket interior and model (modeling the suction assistance installation stage). An axial load cell with a measurement range of 2 kN was used to maintain a constant vertical load during the suction installation stage. Two 5-megapixel machine vision cameras (Allied Vision Technologies Prosilica GC2450C) were positioned opposite the PIV window. As described in Teng et al. (2017) and Ragni et al. (2019), the master camera used an 8-mm lens to

provide a view of the entire window, whereas the micro camera used a 43-mm lens such that the field of view was restricted to the region around the bucket and the effective resolution was approximately 20 times higher. The cameras captured images of the advancing bucket at a frequency of 10 images per mm of bucket penetration. Two LED light panels provided a sufficient and uniform illumination of the PIV window (Teng et al. 2017).

A three-way remotely operated valve (Bienen et al. 2018) on the suction bucket lid [Fig. 2(b)] was used to either allow free flow of fluid across the bucket lid during self-weight installation, or to provide a hydraulic connection to the syringe pump (inner diameter $D_{\text{pump}} = 50$ mm) for suction installation. A 100 kPa Honeywell differential pore-pressure sensor on the bucket lid invert measured the differential pressure across the lid throughout the test.

Soil Sample

As the focus in this paper is the effect of a low permeability clay on suction bucket installation in dense sand, samples were created by combining layers of clay (of near-uniform strength) and dense sand. The properties of the kaolin clay and the fine silica sand used to create the samples are summarized in Tables 2 and 3.

The clay was prepared as a slurry by mixing water and dry kaolin powder at a water content of $\sim 120\%$, before consolidation in a sample container (larger than the PIV sample container) using a hydraulic press under a vertical stress $\sigma'_v = 200$ kPa. The undrained shear strength s_u was assessed from miniature T-bar penetrometer tests performed at single gravity immediately after removing the sample from the hydraulic press. These tests gave an approximately constant $s_u \sim 39$ kPa with depth (adopting a bearing factor, $N_{\text{Tbar}} = 10.5$, Martin and Randolph 2006). After the T-bar penetrometer tests, one of the sample container walls was removed to allow clay slices to be cut from the samples and

Table 2. Silica sand properties

Property	Value
Specific gravity, G_s	2.67
Mean particle size, d_{50} (mm)	0.18
Minimum dry density, ρ_{\min} (kg/m^3)	1,497
Maximum dry density, ρ_{\max} (kg/m^3)	1,774
Minimum void ratio, e_{\min} (-)	0.505
Maximum void ratio, e_{\max} (-)	0.784
Permeability (water saturated), k_w (m/s)	$\sim 1.0 \times 10^{-4}$

Source: Data from Tran (2005); Chow et al. (2019).

Table 3. Kaolin clay properties

Property	Value
Specific gravity, G_s (-)	2.6
Liquid limit, LL (%)	61
Plastic limit, PL (%)	27
Void ratio at $p' = 1 \text{ kPa}$ on CSL, e_{cs} (-)	2.14
Slope NCL, λ (-)	0.205
Slope URL, κ (-)	0.044
Permeability (water saturated), k_w (m/s)	$\sim 1.7 \times 10^{-9}$

Source: Data from Stewart (1992).

placed in the PIV box at the required depth. To quantify the expected undrained shear strength of the clay layer in each test (due to the varying OCR and average vertical effective stress), s_u was calculated using (Ladd et al. 1977):

$$s_u = \sigma'_v (s_u / \sigma'_v)_{NC} \text{OCR}^\Lambda \quad (1)$$

where the vertical effective stress σ'_v was calculated at the mid-depth of each clay layer (i.e., $h_{\text{clay}}/2$ in CoS samples, and $h_{\text{sand}} + h_{\text{clay}}/2$ in SoC samples), the normally consolidated undrained strength ratio was taken as $(s_u / \sigma'_v)_{NC} = 0.15$ (Cocjijn et al. 2014; Morton et al. 2014; O'Beirne et al. 2015), and the plastic volumetric strain ratio was taken as $\Lambda = (\lambda - \kappa)/\lambda$, where λ is the slope of the normal compression line and κ the slope of the unload-reload line. The values of undrained shear strength estimated using Eq. (1) for each clay layer are reported in Table 1.

The sand-over-clay samples (SoC_1, SoC_2; Table 1) involved a clay layer ($h_{\text{clay}} = 70 \text{ mm} = 1.5L$) resting on a 75 mm base layer of very dense coarse sand (to optimize use of the finite amount of overconsolidated clay material). A 30 mm layer of the fine silica sand ($h_{\text{sand}} = 0.6 L$) was air pluviated over the clay into the PIV box using an automated sand rainer and then saturated (details provided later in the paper). The sand layer was sufficiently thick ($h_{\text{sand}} = 0.6 L$) to allow significant suction-assisted penetration in sand to be observed, and investigate any potential changes in seepage flow as the skirt tips approached the clay layer.

The clay-over-sand samples (CoS_1 to CoS_6; Table 1) had a 10-mm-thick drainage layer of coarse sand at the bottom of the PIV box, overlain by a layer of geotextile to promote uniform saturation from the base of the sample. The dense, fine silica sand was created by pluviation (as for the sand-over-clay samples) and then saturated. Finally, a clay layer of thickness $h_{\text{clay}} = 10, 20, \text{ or } 30 \text{ mm}$ (0.2, 0.4, 0.6 L ; refer to Table 1) was placed manually on the sand layer. The motivation for a clay thickness $h_{\text{clay}} = 0.2 L$ was to assess the effect of introducing a hydraulic barrier in the sand at different pumping rates, whereas the effect of clay thickness ($h_{\text{clay}} = 0.4 L$ and $0.6 L$) was assessed at the same pumping rate. All samples had a height of 175 mm (i.e., 3.5 L).

The sand was saturated from the base of the sand layer on the laboratory floor with a solution of water and 1.4% cellulose ether,

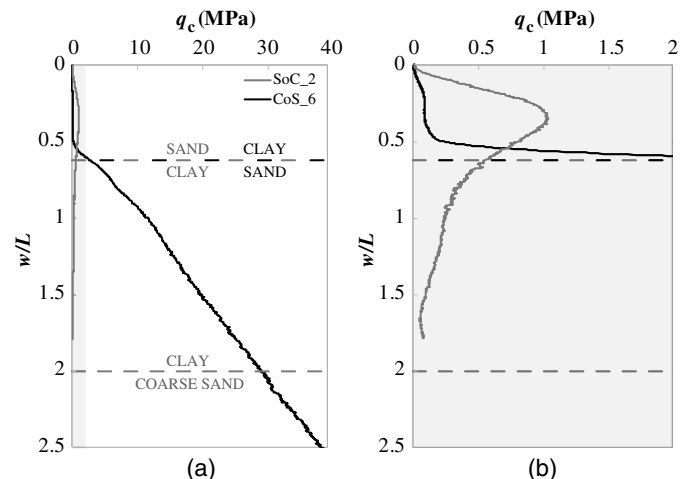


Fig. 3. Representative cone penetration test (CPT) profiles for sand-over-clay (SoC_2, gray) and clay-over-sand (CoS_6, black). (b, RHS) shows an enlarged view of (a, LHS). Clay-sand interfaces reported at actual depth (Table 1).

to obtain a viscosity of 100 cSt (at a temperature of 20°C, DOW 2002). Matching the fluid viscosity with the centrifuge acceleration of 100g allowed the drainage properties to be scaled correctly (Tan and Scott 1985; Taylor 1987; Dewoolkar et al. 1999; Bienen et al. 2018).

In order to obtain the optimal particle contrast required for high-quality PIV analyses, 25% dyed (black) sand was mixed with 75% untreated sand. Contrast in the clay layer was achieved by applying black artificial seeding material to the exposed surface of the (white) clay before placing the layer in the PIV box (with the black and white textured clay surface visible in the photos).

Cone penetrometer tests (CPTs) were performed at the testing centrifuge acceleration of 100g in each sample using a 7 mm diameter cone penetrometer, penetrated at 1 mm/s. Representative profiles of cone tip resistance q_c with depth for sand-over-clay and clay-over-sand samples are provided in Fig. 3, and are considered later in the paper to assist in the interpretation of the measured suction and rate of bucket penetration.

Testing Procedure

A jacked test in a sand-over-clay sample (SoC_1) and in a clay-over-sample sample (CoS_1) with the lid vented was included in the experimental program to provide a basis for comparison with tests in samples with equivalent layering but where suction-assisted installation was employed. The penetration velocity in these jacked tests was 0.057 mm/s, consistent with that adopted in sand tests reported in Ragni et al. (2019).

The remaining suction-assisted installation tests comprised two main stages: (1) initial self-weight penetration, and (2) suction-assisted penetration.

Although self-weight penetration is a load-controlled event in practice, displacement control using the same penetration velocity as in the jacked tests (i.e., 0.057 mm/s) was chosen to facilitate comparison between the tests. A self-weight penetration of $z_{s-w}/L = 0.2$ was adopted for the sand-over-clay case (SoC_2, matching the self-weight embedment in the sand tests reported in Ragni et al. 2019). In clay-over-sand, it was assumed that the bucket self-weight would cause the skirts to penetrate through the clay layer into the underlying sand, regardless of h_{clay} . Hence, the skirts were consistently

Table 4. Summary of experimental results

Test	Self-weight penetration z/L (-)	V_{s-w}/A^a (kPa)	Final penetration z/L (-)	Internal plug heave h_{plug}/L (-)	Skirt contribution to plug heave h_{skirt}/L (-)	Dilation contribution to plug heave h_{dil}/L (-)	Comment
SoC_1	N/A (Jacked)	N/A (Jacked)	1.11	-0.13	N/A	N/A	Final penetration, $z/L > 1$ due to significant compression of the bottom clay layer
SoC_2	0.2	99.0	1.19	-0.23	N/A	N/A	
CoS_1	N/A (Jacked)	N/A (Jacked)	0.95	0.05	0.09	-0.04	
CoS_2	0.3	357.3	0.70	0.14	0.10	0.04	Full installation not achieved due to insufficient suction generation at this low pumping rate
CoS_3	0.3	384.3	0.80	0.17	0.12	0.05	Final penetration + internal plug heave, $z/L + h_{\text{plug}}/L < 1$ due to clay plug fracture and minor water gap at the clay-sand interface
CoS_4	0.3	303.4	0.72	0.14	0.10	0.04	Full installation not achieved due to sudden failure of the soft sealant at the model-window interface
CoS_5	0.5	438.7	0.86	0.13	0.11	0.02	Final penetration + internal plug heave, $z/L + h_{\text{plug}}/L < 1$ due to minor water gap at the clay-sand interface
CoS_6	0.7	906.4	0.92	0.09	0.10	-0.01	

^a $A = (\pi D_i^2/8)$, the internal plan area of the half-suction bucket.

jacked $\Delta z/L = 0.1$ into the sand layer, such that the suction-assisted installation commenced at the same embedment depth (relative to the top of the sand layer).

Once the target self-weight embedment was achieved (Table 4), the actuator was switched to load control to maintain the vertical load V_{s-w} (measured at the end of the self-weight installation phase, see Table 4) during the suction-assisted installation phase of the test. The valve was then adjusted to hydraulically connect the bucket to the syringe pump, which was then activated at a constant pumping flow rate q_{pump} (see Table 1 for the pumping flow rates adopted in each test). As discussed in Bienen et al. (2018), the penetration rate at model scale with the pore fluid viscosity matching the centrifugal acceleration corresponds to that in the prototype with water as a pore fluid, such that the overall installation duration is realistic. The average pumping flow rate was thus selected to achieve a realistic installation duration, and then varied to investigate the effect that this might have on the soil response during suction bucket installation.

The entire test sequence was performed at 100g without stopping the centrifuge.

PIV Post-Analysis

PIV analyses were performed using GeoPIV-RG (Stanier and White 2013; Stanier et al. 2016) on the high-resolution images obtained using the micro camera [field of view shown in Fig. 2(c)] at different normalized depths z/L and for an incremental bucket penetration $\Delta z = 0.5$ mm.

The array used to analyze the soil domain was formed using 50-pixel square subsets equally spaced every 25 pixels (i.e., with initial overlapping of 25 pixels). The automatic reference image updating scheme described in Stanier et al. (2016) was utilized to automatically track the soil displacements throughout the whole image series, while ensuring maximal correlations with the adoption of stringent convergence criteria. All the PIV analyses adopted a minimum correlation coefficient tolerance, $CC_{ZNCC} = 0.75$ [as recommended in Stanier et al. (2016), where 0 = no correlation and 1 = perfect correlation].

Results and Discussion

Table 4 summarizes the main results from the tests, including the embedment achieved after each installation stage, the contribution (to the final embedment) of plug heave and the volume of soil displaced by the advancing skirts. Complete embedment was not achieved in every test as noted in the comments in Table 4. Further details and interpretation of these results, including observations from the PIV analyses, are provided in the following sections.

Sand-Over-Clay

Deformation Mechanisms and Changes in Soil State

Figs. 4 and 5 show the total shear γ_s (LHS) and total volumetric ε_v strain distribution (RHS; positive = compression) for jacked (Fig. 4) and suction-assisted installation (Fig. 5) in sand-over-clay (SoC_1, SoC_2) due to incremental penetrations of $\Delta z = 0.5$ mm at increasing depths, $z_{\text{PIV}}/L = 0.3, 0.6$ and 0.9.

The two cases are similar initially ($z/L \leq 0.3$), with prevalent shearing along the skirt, and below the skirt tips. In the case of suction-induced installation, inverted V shear bands propagate towards the inside of the bucket [Fig. 5(a)], similar to observations from installation in dense sand (Ragni et al. 2019). However, as penetration advances and the skirt tips reach the sand-clay interface ($z_{\text{PIV}}/L = 0.6$), the underlying clay layer deforms. As the clay has a lower strength than the overlying sand, the inverted V shear bands disappear and rapid advancement of the bucket is observed, which is accompanied by localized shear strains along the skirts [Figs. 4(b and c); 5(b and c)].

The above behavior is reflected in the volumetric strain distributions, where the majority of the sand plug does not undergo any significant change throughout the installation. Minor compression is observed under the skirt tips at $z_{\text{PIV}}/L = 0.3, 0.6$ [Figs. 4(d and e); 5(d and e)], whereas compression of the clay material is more visible at $z_{\text{PIV}}/L = 0.9$ [Figs. 4(f) and 5(f)]. The sand-clay interface experiences significant deformation, as also documented for other foundations penetrating through sand over clay, with a sand frustum being pushed ahead of the foundation into the clay [Meyerhof (1974)].

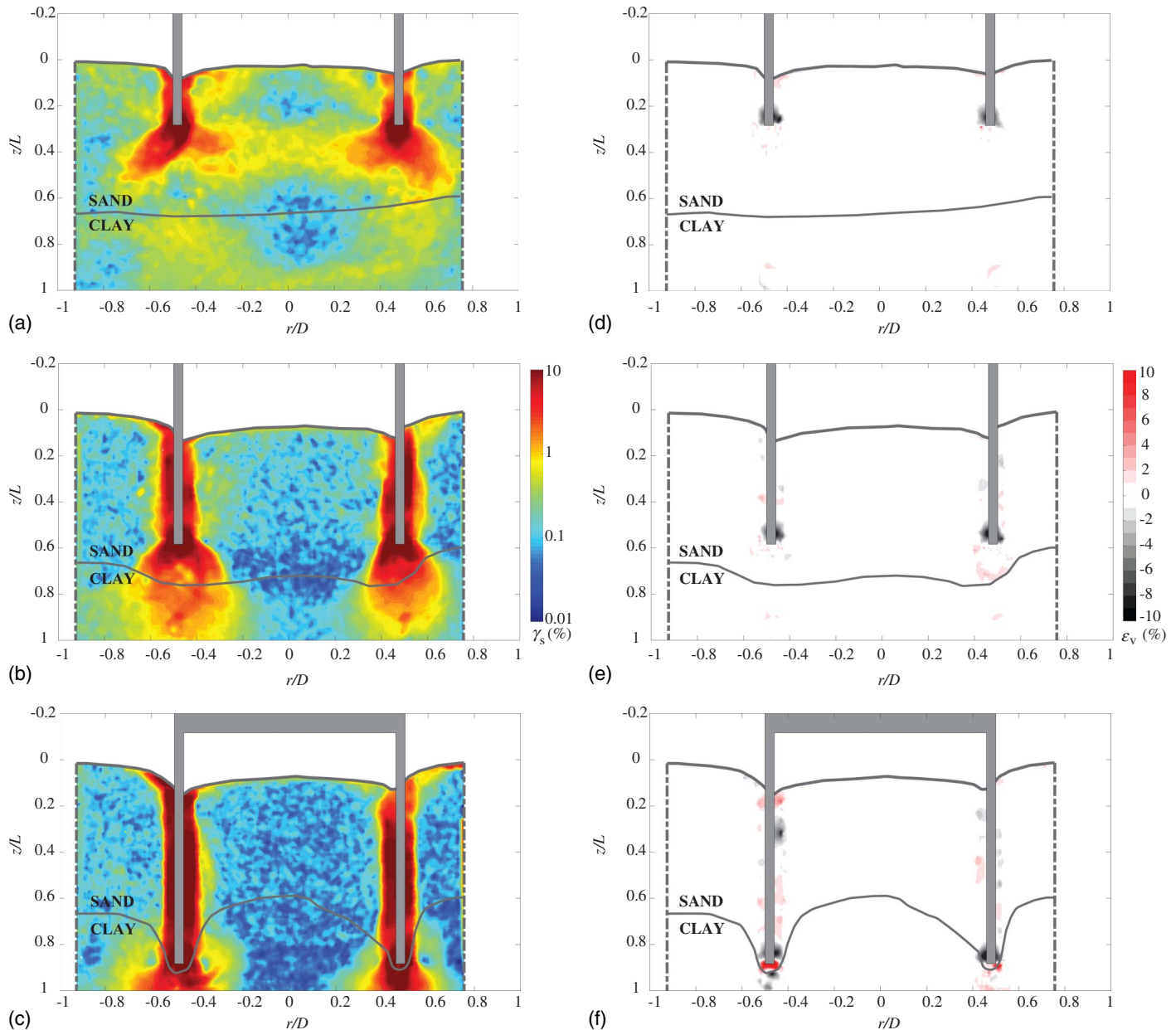


Fig. 4. Total shear strain γ_s (%) (LHS; a,b,c) and total volumetric strain ε_v (%) (RHS, compression positive; d,e,f) contours during jacked installation (SoC_1) at increasing normalized depth $z_{\text{PIV}}/L = 0.30$ (a,d); 0.60 (b,e); and 0.90 (c,f).

on shallow footings; and Craig and Chua (1990), Teh et al. (2008), Qiu and Grabe (2012) and Lee et al. (2013), among others, on spudcan foundations]. However, unlike these examples, in these bucket penetration experiments the sand is pushed down by the skirt tips rather than the entire foundation cross-section. An important consequence is that the bucket skirts did not come in contact with the clay layer. Thus, it can be deduced that for the suction-assisted case (SoC_2) the seepage flow was never fully blocked. Differences in radial stresses induced by jacked and suction-assisted installation, respectively, are reflected in the soil strain and deformation fields (comparing Figs. 4 and 5).

Suction and Penetration Rate Profiles

The normalized suction pressure $p/\gamma'_s D$ (where γ'_s is the submerged unit weight of the sand) measured at the lid invert in SoC_2 [Fig. 6(a)] increased during the initial penetration stage [consistently with development of V shear bands in Fig. 5(a)],

but reduced as the sand-clay interface was approached. The normalized penetration rate of the bucket, $(\dot{z}A)_{\text{bucket}}/q_{\text{pump}}$ [Fig. 6(b)], where A is the internal cross-sectional area of the half-model bucket $= \pi D_l^2/8$ initially reduces ($z/L \leq 0.4$) due to the constant applied pumping flow rate despite increasing penetration resistance in the sand layer, but then increases as the skirts approach and penetrate through the clay layer.

According to the theory of volume continuity, the fluid volume pumped out by the syringe pump Vol_{pump} should equal the sum of (1) the volume of water displaced by the penetrating bucket Vol_{bucket} , (2) the seepage volume Vol_{seep} , (3) and a system volume due to water compressibility Vol_{sys} (usually negligible):

$$Vol_{\text{pump}} = Vol_{\text{bucket}} + Vol_{\text{seep}} + Vol_{\text{sys}} \quad (2)$$

The theory is valid provided the increasing bucket penetration resistance is continuously overcome through the generation of suction. Furthermore, if the clay layer prevents seepage

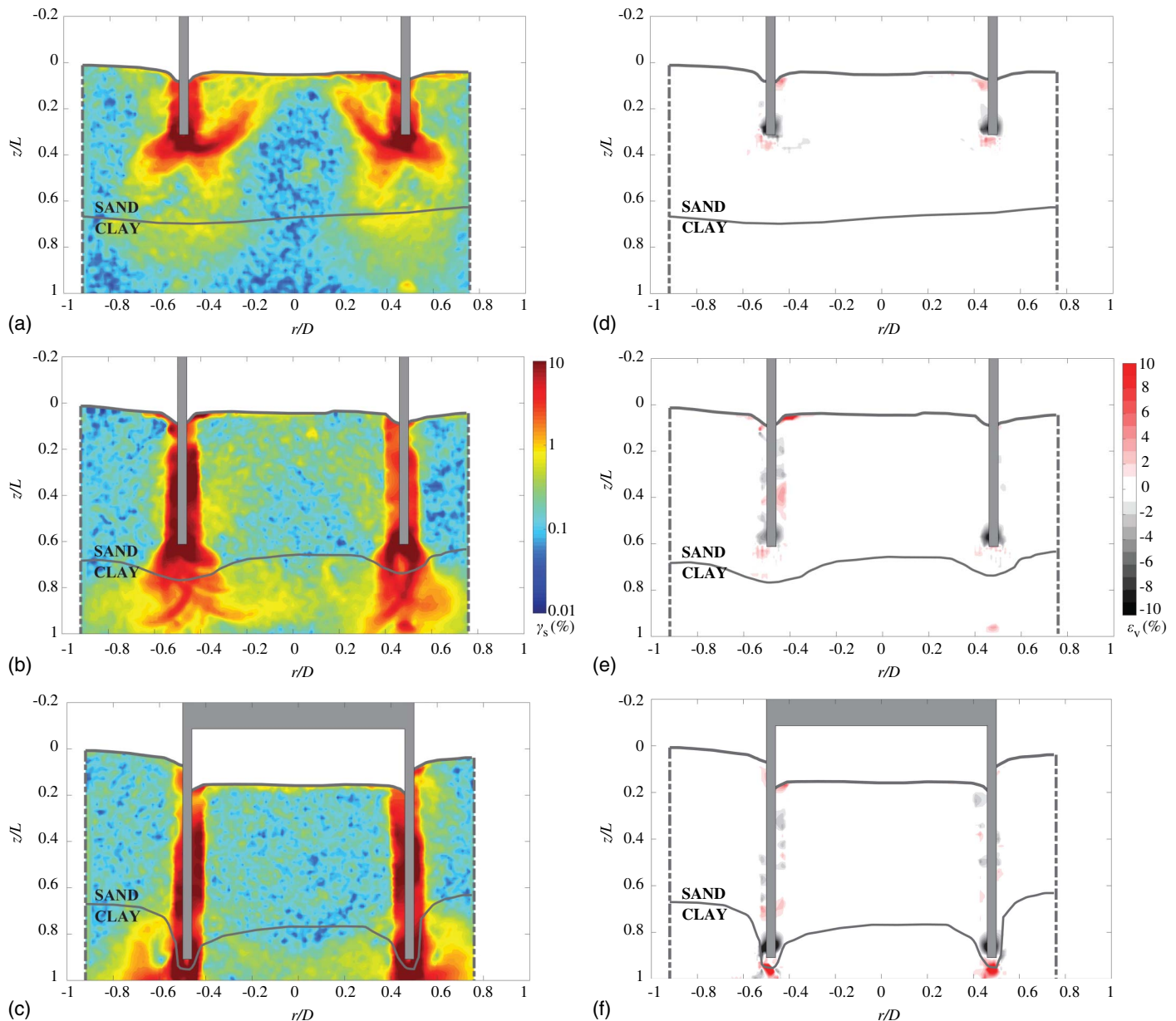


Fig. 5. Total shear strain (%) (LHS; a,b,c) and total volumetric strain (%) (RHS; d,e,f) contours during suction-assisted installation (SoC_2) at increasing normalized depth: $z_{\text{PPV}}/L = 0.30$ (a,d); 0.60 (b,e); and 0.90 (c,f).

(i.e., $Vol_{\text{sep}} = 0$), the normalized penetration rate should be constant and equal to unity.

However, for SoC_2 the normalized penetration rate, $(\dot{z}A)_{\text{bucket}}/q_{\text{pump}} > 1$ in the clay layer (for $z/L > 0.6$). The CPT profile [Fig. 3(b)] offers an explanation in this regard, showing that the cone tip resistance, q_c , at the bucket self-weight embedment ($z_{\text{s-w}}/L = 0.2$) is larger than in the clay (q_c at $0.6 < z/L < 1$). This suggests that the bucket self-weight $V_{\text{s-w}}$ would be sufficient to penetrate through the clay layer. However, an extra vertical driving force pA is still being provided through the application of suction ($p/\gamma'_s D > 0$) which, in combination with $V_{\text{s-w}}$, causes the bucket penetration rate to exceed the pumping flow rate [$(\dot{z}A)_{\text{bucket}}/q_{\text{pump}} > 1$].

This results in overpressure (rather than suction) in the inner compartment ($p/\gamma'_s D < 0$ at $z/L \sim 0.7$), because the volume of fluid displaced by the advancing bucket is greater than the volume pumped by the syringe, causing the penetration rate to decrease

again. The soil plug responds in an undrained fashion, such that the suction bucket and soil plug behave much like a rigid embedded foundation, transferring the failure mechanism to the skirt tip level (Fig. 7, SoC_2, macro camera view to fully capture the mechanism). A different response is observed in Fig. 8 for the jacked installation (SoC_1, macro camera view), as the free flow of fluid resulted in a different drainage response within the soil plug. At $z/L \sim 1.15$, equilibrium between the resultant vertical force ($V_{\text{sw}} + pA$) and the bucket resistance is achieved for SoC_2 (i.e., $p/\gamma'_s D = 0$), followed shortly by contact of the lid with the soil surface at $z_{\text{fin}}/L = 1.19$. The jacked installation (SoC_1) achieved lid contact at $z_{\text{fin}}/L = 1.11$ (Table 4).

Summary, Sand-Over-Clay

In summary, the results of the installations in sand-over-clay are in line with the expected behavior (considering the CPT profiles),

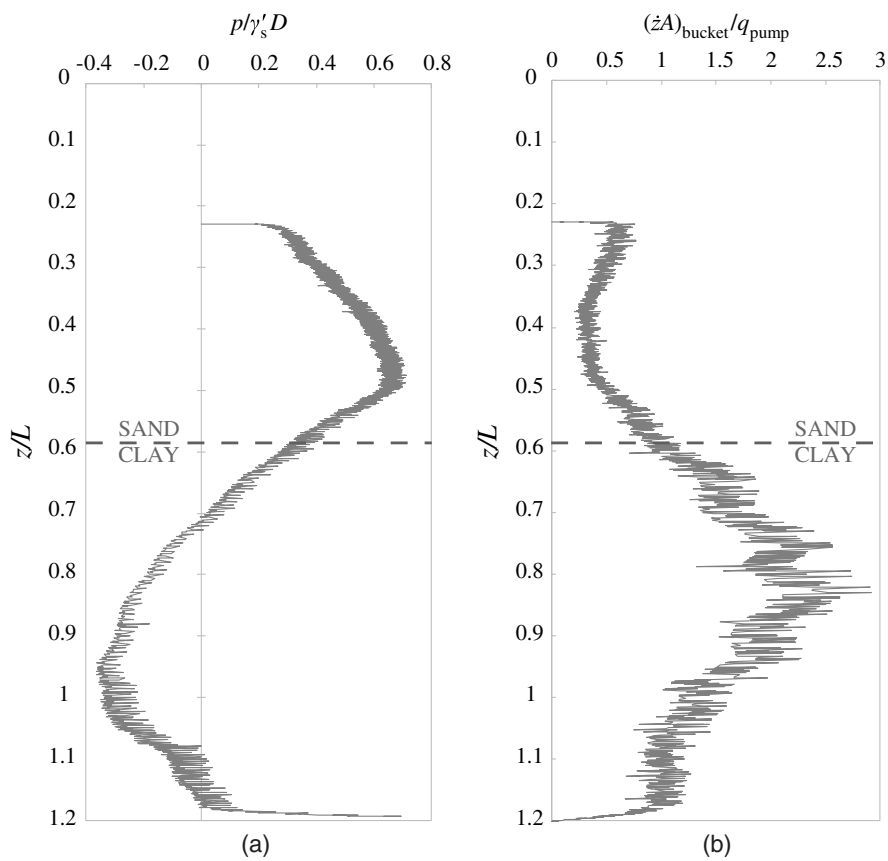


Fig. 6. (a) Normalized suction pressure (p equivalent to p_1 of Fig. 1); and (b) normalized penetration rate profiles for SoC_2. Sand-clay interface reported at actual depth (see Table 1).

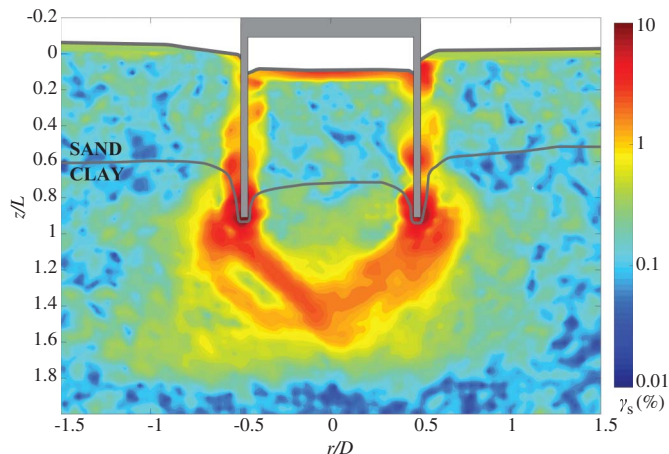


Fig. 7. Total shear strain (%) contours during suction-assisted installation (SoC_2) at normalized depth $z_{\text{PIV}}/L = 0.90$; obtained with macro camera (to fully capture the mechanism) images.

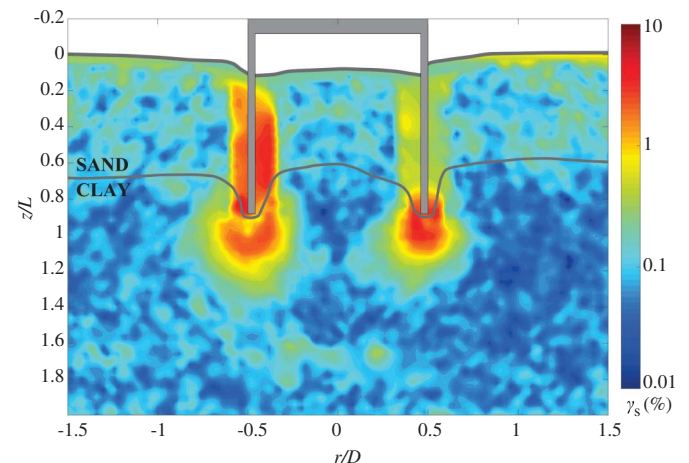


Fig. 8. Total shear strain (%) contours during jacked installation (SoC_1) at normalized depth $z_{\text{PIV}}/L = 0.90$; obtained with macro camera (to fully capture the mechanism) images.

with suction-assisted installation (SoC_2) proving to be unproblematic for the test conditions considered. The final penetration depth was greater than the skirt lengths for both jacked and suction-assisted installations ($z_{\text{fin}}/L = 1.11$ and 1.19 , Table 4), which is consistent with the downward migration of the sand-clay interface. Further effort in sand-over clay seabed profiles should focus on establishing if installation is also straightforward for higher clay strengths (as lower sand densities are likely to be less problematic).

Clay-Over-Sand

Deformation Mechanisms

Fig. 9 shows the progression of the deformation mechanism (resultant displacement contours) associated with the jacked installation in clay over sand (CoS_1, $h_{\text{clay}} = 0.2L$). At $z_{\text{PIV}}/L = 0.15$ [Fig. 9(a)] a shallow mechanism is observed within the clay layer. Clay material is squeezed laterally as the skirts approach the

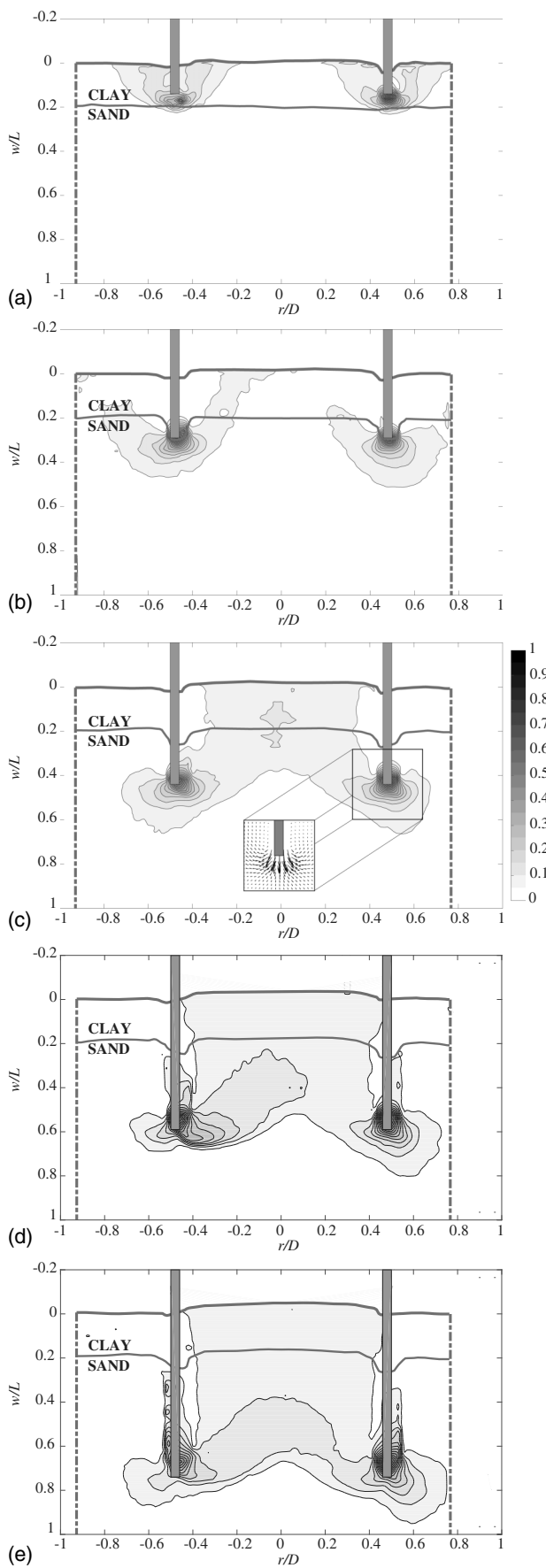


Fig. 9. Normalized resultant displacement contours during jacked installation in test CoS_1 at increasing normalized depth: (a) $z_{\text{PIV}}/L = 0.15$; (b) 0.30; (c) 0.45; (d) 0.60; and (e) 0.75.

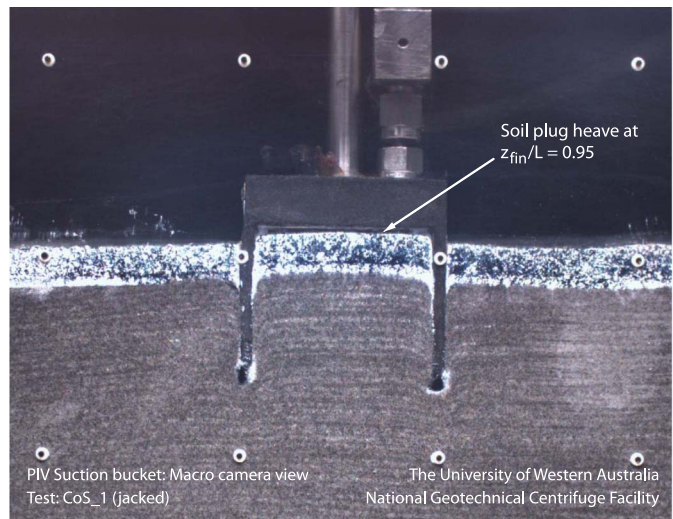


Fig. 10. Final soil plug heave in test CoS_1 (jacked) at $z_{\text{fin}}/L = 0.95$.

stronger underlying sand. As penetration continues into the sand [$z_{\text{PIV}}/L = 0.30$; Fig. 9(b)], a transition to a more localized mechanism around the skirt tips is observed, in line with observations from Ragni et al. (2019) for installation in dense sand.

During jacked installation, the soil displaced by the skirt tips is equally distributed inside and outside the bucket [see inset in Fig. 9(c)]. The final soil plug heave $h_{\text{plug}}/L \sim 0.05$ recorded at the final penetration of $z_{\text{fin}}/L = 0.95$ (Fig. 10) can be therefore attributed to the soil displaced by the advancing skirts entering the bucket (quantified in $h_{\text{skirt}}/L \sim 0.09$, Table 4), rather than dilation of the dense sand. In fact, the definition of a dilation contribution, $h_{\text{dil}}/L = (h_{\text{plug}} - h_{\text{skirt}})/L = -0.04$, reveals that the sand might have undergone some minor contraction in volume.

Fig. 11 shows the suction-assisted installation with medium pumping flow rate ($q_{\text{pump}} = 235.62 \text{ mm}^3/\text{s}$, CoS_3) in terms of normalized displacement contours [LHS, Figs. 11(a–c)] and total shear strain distribution [RHS, Figs. 11(d–f)]. In the early stages of suction-assisted penetration ($0.3 < z/L < 0.45$), the clay layer significantly reduces seepage flow, and suction simply creates an additional vertical driving force p_A . The absence of seepage flow through the underlying sand plug translates to an approximately constant normalized penetration rate $(zA)_{\text{bucket}}/q_{\text{pump}}$ [Fig. 12(b)]. Assuming there is no seepage flow, the normalized penetration rate should be equal to unity (Bienen et al. 2018), although in this case it is slightly lower, which indicates that there is either minor seepage through the clay layer or other losses in the system. However, this is of no real consequence as the purpose of Fig. 12 is to assess relative comparisons between tests.

However, at $z_{\text{PIV}}/L = 0.45$ [Figs. 11(a and d)], the formation of a gap at the clay-sand interface can be observed, which spells the beginning of the clay plug uplift. The suction pressure required to lift the plug, $p_1 = p_{\text{plug}}$ [Fig. 1(b)], can be calculated by Senders et al. (2007):

$$p_{\text{plug}} = (\gamma'_c + 4/D_i \alpha s_u) h_{\text{clay}} \quad (3)$$

where $\gamma'_c = 7.5 \text{ kN/m}^3$ is the submerged unit weight of the clay, $D_i = 46 \text{ mm}$ is the internal diameter of the model bucket, and α is the interface friction ratio (selected as the inverse of the sensitivity [Andersen et al. 2005], i.e., $\alpha = 0.4$). The theoretical value—adjusted for the half-model geometry in these tests—of $p_{\text{plug}}/(\gamma'_s D) = 0.27$ underestimated the experimental $p/\gamma'_s D \sim 0.50$ for

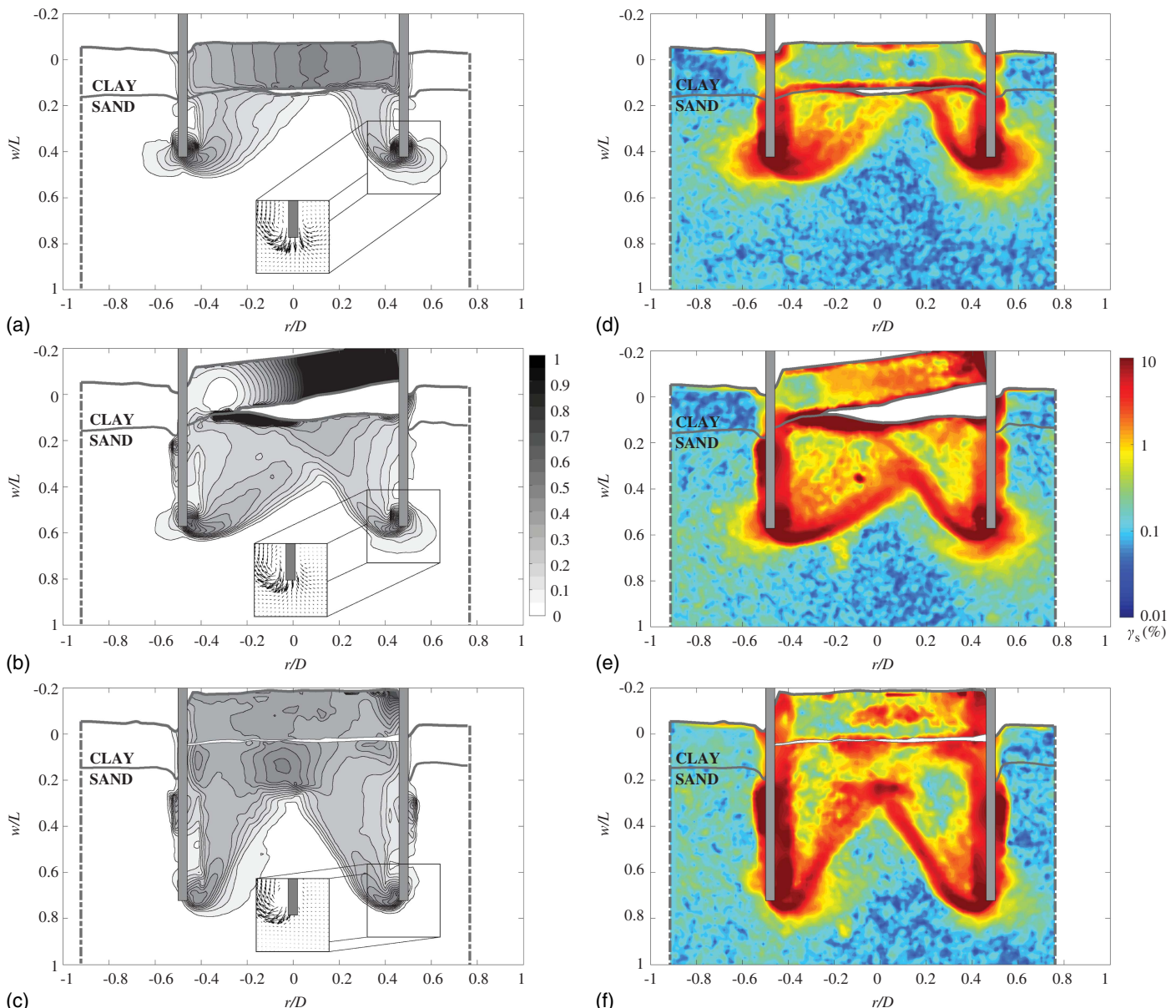


Fig. 11. Normalized resultant displacement (LHS) and total shear strain (%) (RHS) contours during suction-assisted installation in test CoS_3 ($h_{\text{clay}} = 0.2L$, $q_{\text{pump}} = 235.6 \text{ mm}^3/\text{s}$) at increasing normalized depth: (a–d) $z_{\text{PIV}}/L = 0.45$; (b–e) 0.60; and (c–f) 0.75.

CoS_3 at $z/L = 0.46$ [Fig. 12(a)], when complete propagation of the fracture was observed (Fig. 13). On one hand, such difference can be explained by the uncertainties related to the homogeneity of the clay layer in terms of strength and thickness, as well as the assumed value of $\alpha = 0.4$. On the other hand, the difficulty associated with the identification of the exact moment when the fracture fully propagates (which occurs extremely rapidly in a centrifuge environment) in the experiment should be considered.

As explained in Senders et al. (2007), any increase in p_1 above p_{plug} translates to suction [$p_2 = p_1 - p_{\text{plug}}$, Fig. 1(b)] and the generation of seepage flow in the sand. Given the constant pumping flow rate applied in the experiments, this results in a reduction in the penetration rate $(\dot{z}A)_{\text{bucket}}/q_{\text{pump}}$ [Fig. 12(b)]. Associated with the opening of the gap at the clay-sand interface is an irregular overburden pressure acting on the underlying sand, which causes the asymmetric deformation mechanism [evident in Figs. 11(a and b)].

At $z_{\text{PIV}}/L = 0.60$ [Figs. 11(b and e)], the gap has visibly developed. Rather than moving upwards, as postulated by Senders et al.

(2007), the clay plug is rotating, which is likely due to asynchronous failure at the clay-skirt interface.

As the clay plug rotates, a fluid channel eventually opens along the right-hand-side skirt (Fig. 14), such that a differential pressure between the lid invert and the surface of the sand layer (i.e., $p_1 - p_2$) no longer exists. At $z_{\text{PIV}}/L = 0.75$ [Figs. 11(c and f)], the clay plug comes to rest on the underlying sand (although a minor gap is still visible), since the pressure p_2 has been dissipated. The deformation mechanism is now symmetric, and the installation can be compared to a sand-only case (Ragni et al. 2019).

Changes in Soil State

Fig. 15 presents the total volumetric strain distribution for the installation performed with a medium pumping flow rate ($q_{\text{pump}} = 235.62 \text{ mm}^3/\text{s}$, CoS_3). Initially [$z_{\text{PIV}}/L = 0.45$, Fig. 15(a)], the absence of any relevant volumetric expansion in the sand plug is consistent with the extremely low expected seepage flow (i.e., minimal p_2). The minimal plug heave development is consistent with the

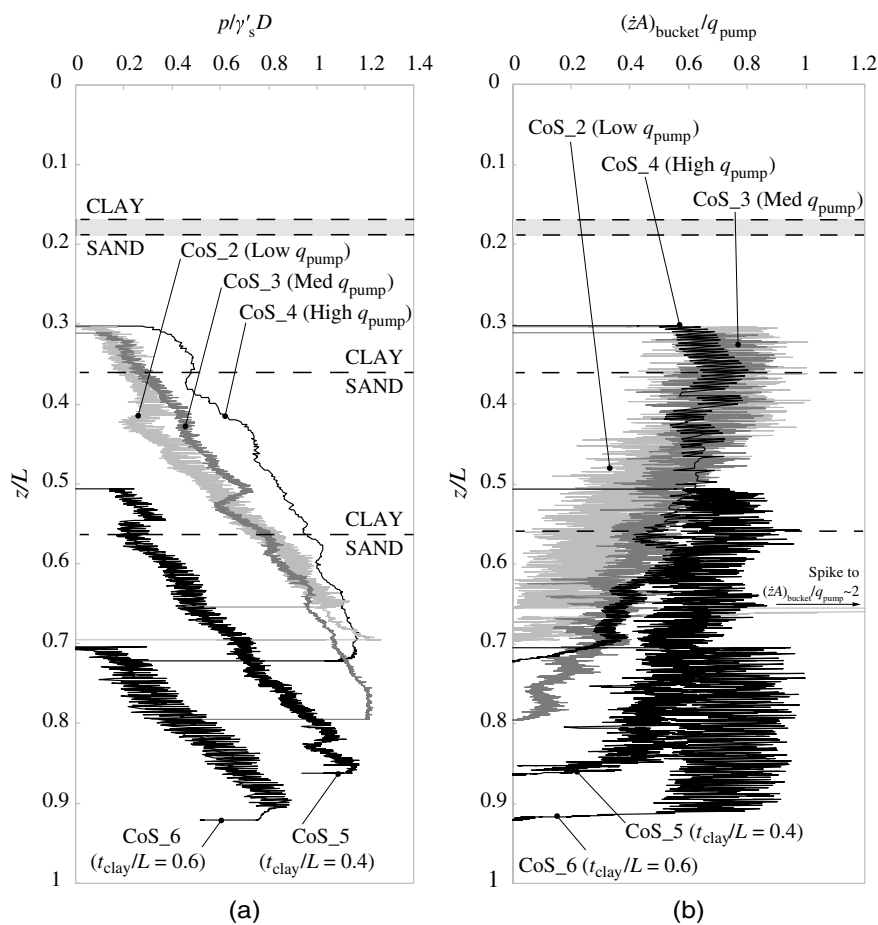


Fig. 12. (a) Normalized suction pressure (p equivalent to p_1 of Fig. 1); and (b) normalized penetration rate profiles for clay-over-sand (CoS) tests. Clay-sand interfaces reported at actual depth (Table 1).

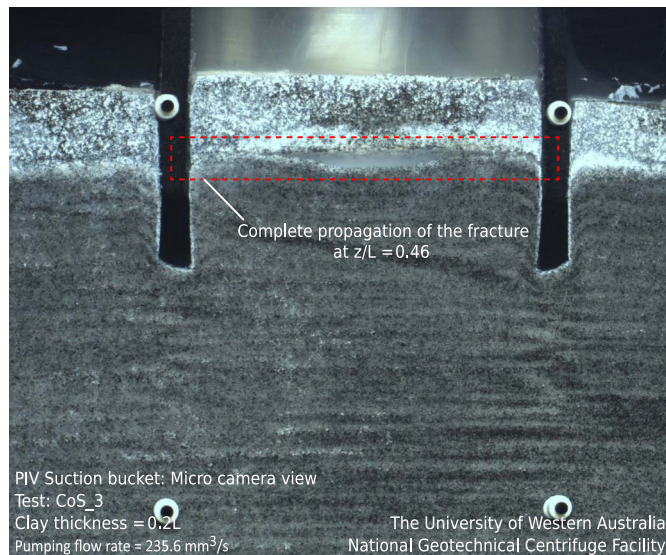


Fig. 13. Complete propagation of the fracture at the sand-clay interface in test CoS_3 (medium pumping flow rate) during suction-assisted installation at $z/L = 0.46$.

observed negligible sand dilation, and the amount of soil entering the bucket [inset Fig. 11(a), comparable to inset Fig. 9(c) for the jacked installation]. Significant dilation is observed across the clay-sand interface, flagging an imminent fracture.

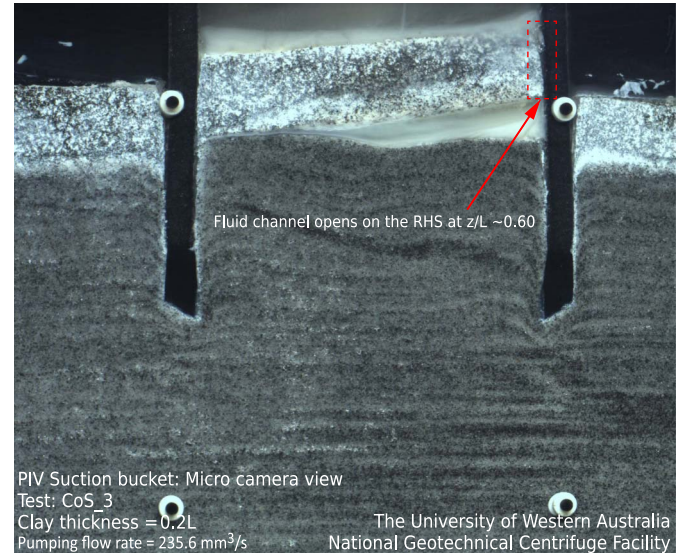


Fig. 14. Opening of a fluid channel along the RHS skirt in test CoS_3 (medium pumping flow rate) during suction-assisted installation at $z/L \sim 0.6$.

As penetration continues [$z_{\text{PIV}}/L = 0.60, 0.75$; Figs. 15(b and c)], volumetric expansion is experienced at the crown of the inverted V mechanism within the sand plug. A plug heave $h_{\text{plug}}/L = 0.17$ at the final penetration $z_{\text{fin}}/L = 0.8$ was

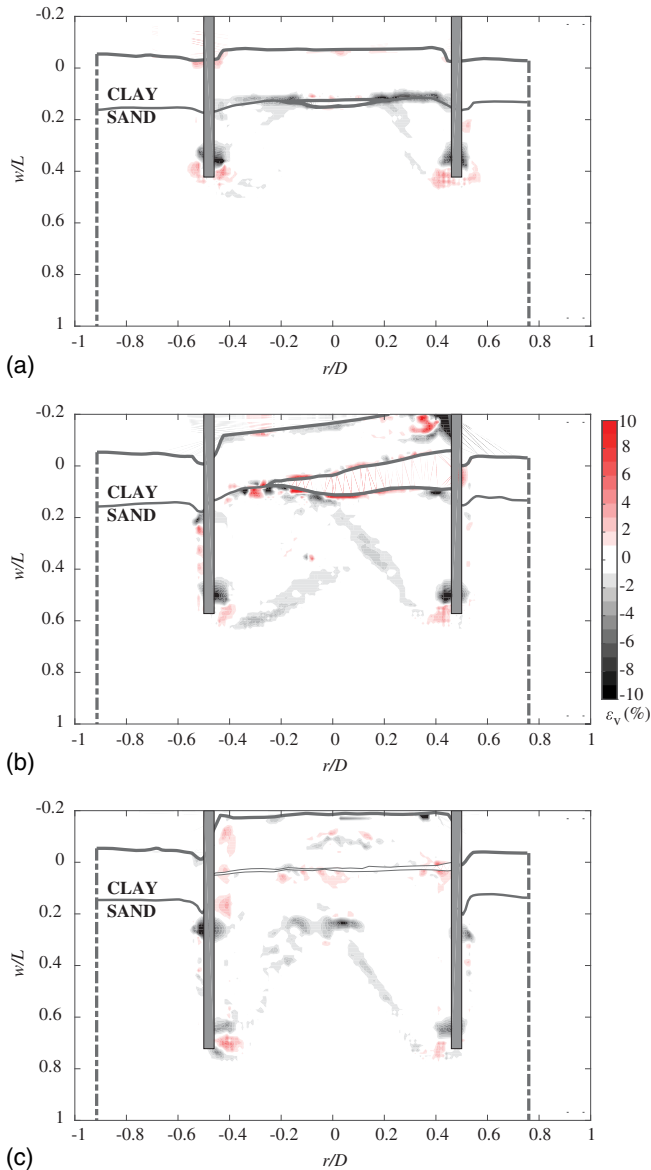


Fig. 15. Total volumetric strain (%) contours during suction-assisted installation in test CoS_3 at increasing normalized depth: (a) $z_{\text{PIV}}/L = 0.45$; (b) 0.60; and (c) 0.75.

recorded (Fig. 16). The equivalent volume of soil displaced by the skirts at $z_{\text{fin}}/L = 0.8$ that entered the bucket is quantified as $h_{\text{skirt}}/L = 0.12$ (assuming that all the soil displaced by the skirts enters the bucket during suction-assisted installation, but only half during self-weight installation; see insets Fig. 11). Thus, it can be concluded that a limited contribution to plug heave arises from sand dilation (estimated in $h_{\text{dil}}/L = (h_{\text{plug}} - h_{\text{skirt}})/L = 0.05$), as a result of seepage flow and shearing of the sand along the skirts. These contributions can be used to estimate the dilation experienced by the sand layer, since the volumetric strains can be approximated as $\varepsilon_v \sim h_{\text{dil}}/z_{\text{fin}} = 6\%$. Although qualitatively comparable to installations in sand only (Ragni et al. 2019), in the layered soil the limited seepage flow ($p_2 \sim 0$ in the early stage of suction-assisted installation) prevented sustained critical gradients and localized piping from developing, leading to lower final volumetric strains than in sand only [which were in the range of 8%–11%, Ragni et al. 2019].

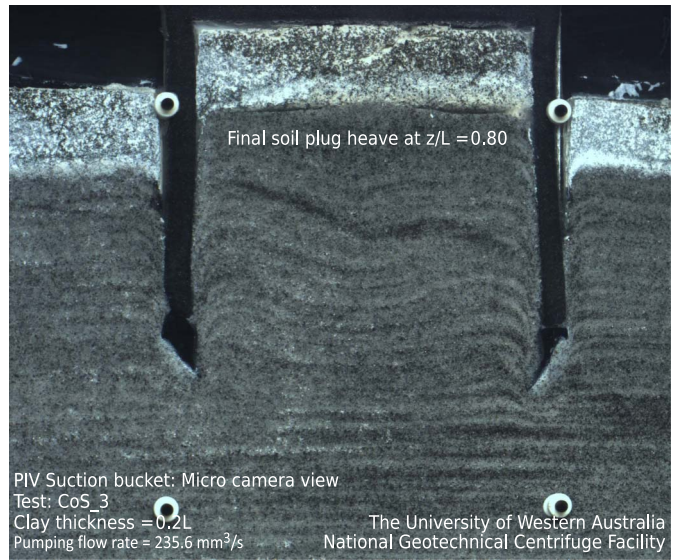


Fig. 16. Final soil plug heave in test CoS_3 (medium pumping flow rate) at $z_{\text{fin}}/L = 0.8$.

Effect of Pumping Flow Rate

The effect of pumping flow rate on suction bucket installation in clay-over-sand was investigated in three tests (CoS_2, 3, 4) across which the pumping flow rate was varied by one order of magnitude ($q_{\text{pump}} = 117.81, 235.62, 1,178.1 \text{ mm}^3/\text{s}$). Generally, higher pumping flow rates led to larger and faster (in absolute terms of penetration rate, \dot{z}) penetration, as already reported in Ragni et al. (2019) for installation in sand. Although the test with the highest pumping flow rate (CoS_4) stopped at $z_{\text{fin}}/L = 0.72$ due to sudden failure of the soft sealant at the model-window interface, extrapolating the normalized penetration rate [Fig. 12(b)] suggests that installation would have continued until the lid made contact with the soil plug.

Fig. 17 compares the soil resultant displacement contours for the three tests with increasing q_{pump} [CoS_2, 3, 4 in Figs. 17(a–c) respectively] at $z_{\text{PIV}}/L = 0.60$. A different clay plug response is observed in each test: uplift for low q_{pump} [CoS_2, Fig. 17(a)], rotation for medium q_{pump} [CoS_3, Fig. 17(b)], and combined uplift/rotation for high q_{pump} [CoS_4, Fig. 17(c)]. This may be influenced by slight inhomogeneities in the soil properties and geometry of the clay plug. The deformation mechanisms in sand appear to be affected by the different clay plug response. Partial plug contact with the sand [CoS_3, Fig. 17(b)] results in the most pronounced asymmetry, as this is likely to provide an irregular overburden pressure, which contrasts with the other two cases.

A much larger clay plug uplift was observed in the test with the lowest pumping flow rate [CoS_2, Fig. 17(a)]. This is in agreement with Senders (2008), who demonstrated that a slow installation process (and a high permeability ratio $k_{\text{sand}}/k_{\text{clay}}$) can increase the plug uplift, as the water inflow inside the gap will determine the extent to which the clay plug is uplifted. Although high q_{pump} generates higher suction in the gap, $p_2 = p_1 - p_{\text{plug}}$ ($p_{2,\text{high}} = 1.32 p_{2,\text{low}}$), the resulting installation process is too fast for a large volume of water, Vol_{seep} , to be drawn into the gap. Assuming that the test with high pumping flow rate has an initial penetration rate that is 10 times higher than the test with low pumping flow rate, the seepage volume for the former case is estimated as ~13% of the latter.

Uplift of the clay plug in CoS_2 (low q_{pump}) progressed until the bucket lid touched the plug. At this point, direct contact between the clay plug and the valve interrupted the flow (Fig. 18), causing a

reduction in suction that allowed the plug to collapse on the underlying sand. The event is clearly visible in Fig. 12(a) at $z/L = 0.66$. However, interruption of flow, represented by the drop in $p/\gamma'_s D$, did not result in premature termination of the penetration. Rather, the plug collapse allowed for a sudden increase in suction pressure from p_2 to $p_2 + p_{\text{plug}}$, resulting in a spike in the normalized penetration rate to $(\dot{z}A)_{\text{bucket}}/q_{\text{pump}} \sim 2$. However, full installation could not be achieved, as the increased seepage flow in the sand quickly resulted in refusal of the suction bucket at $z_{\text{fin}}/L = 0.70$ [Fig. 12(b)], similar to Ragni et al. (2019) for tests in dense sand at a low pumping rate.

Effect of Clay Layer Thickness

The effects of a thicker clay layer ($h_{\text{clay}} = 0.4, 0.6 L$) on suction bucket installation were investigated in CoS_5 and CoS_6. Suction-assisted penetration commenced when the skirts penetrated 0.1 L into the sand layer (i.e., $z_{\text{s-w}}/L = 0.5$ and 0.7 for CoS_5 and

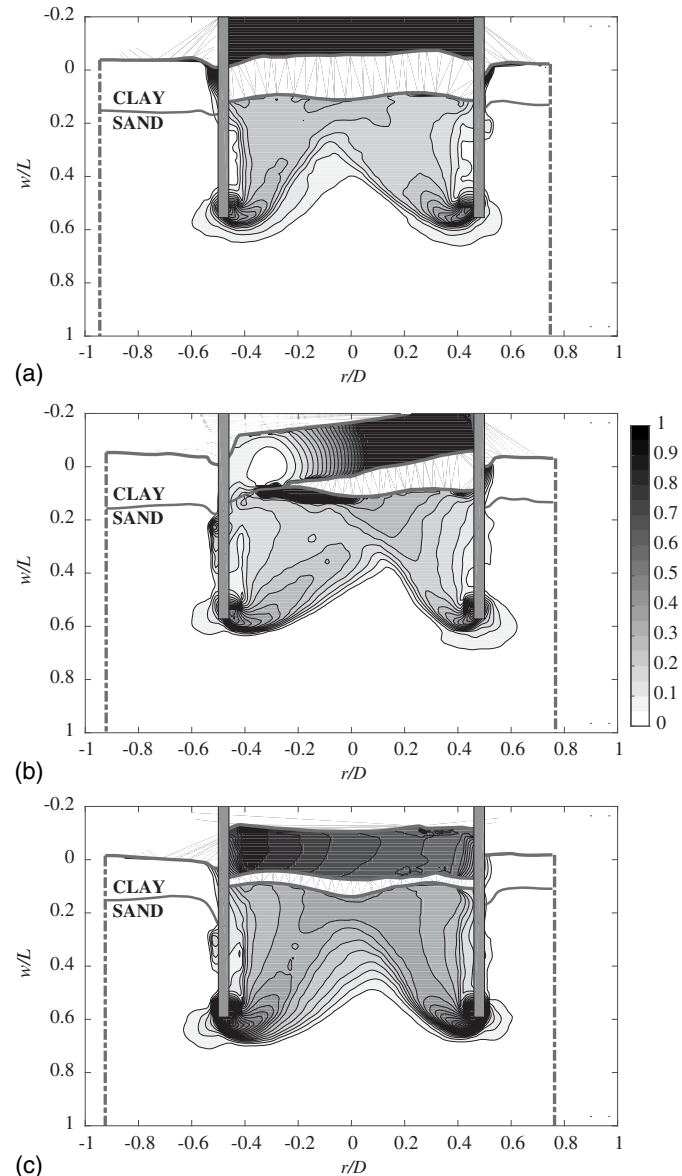


Fig. 17. Normalized resultant displacement contours during suction-assisted installation at normalized depth $z_{\text{PIV}}/L = 0.60$ for increasing pumping flow rate: (a) $117.8 \text{ mm}^3/\text{s}$ (CoS_2); (b) $235.6 \text{ mm}^3/\text{s}$ (CoS_3); and (c) $1,178.1 \text{ mm}^3/\text{s}$ (CoS_4).

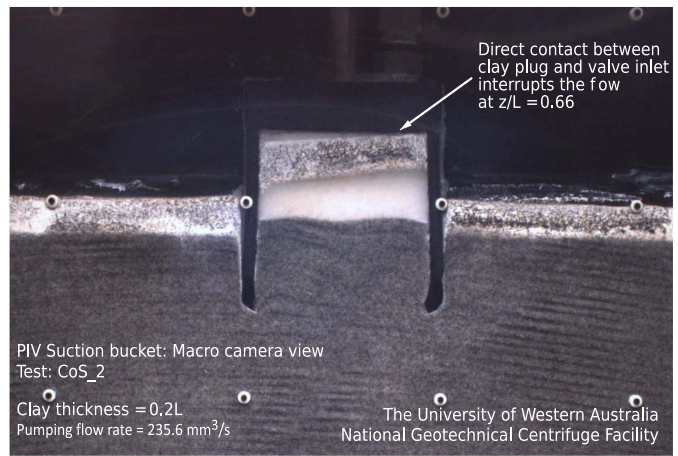


Fig. 18. Direct contact between clay plug and valve inlet causing interruption of the flow during suction-assisted installation in test CoS_2 (low pumping flow rate) at $z/L = 0.66$.

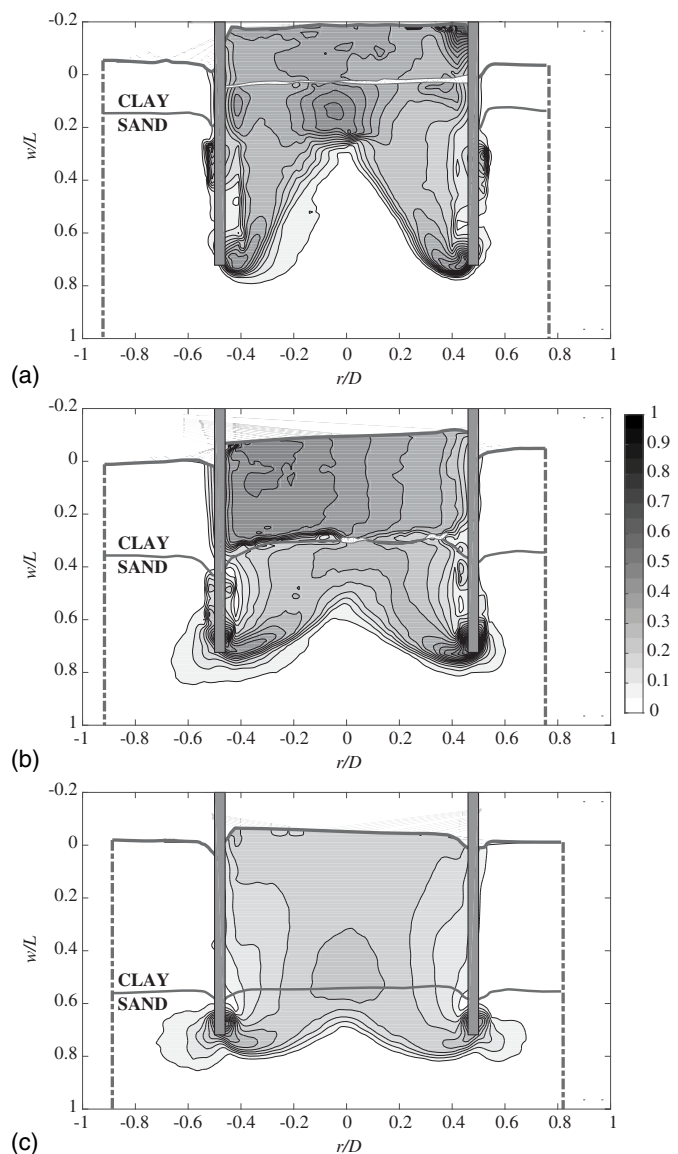


Fig. 19. Normalised resultant displacement contours during suction-assisted installation at normalized depth $z_{\text{PIV}}/L = 0.75$ for increasing clay thickness h_{clay}/L : (a) 0.2 (CoS_3); (b) 0.4 (CoS_5); and (c) 0.6 (CoS_6).

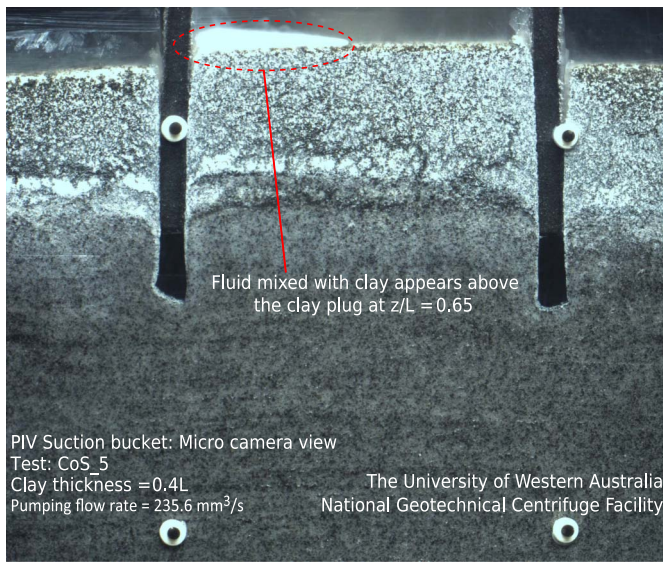


Fig. 20. Fluid mixed with clay appears above the clay plug during suction-assisted installation in test CoS_5 at $z/L = 0.65$.

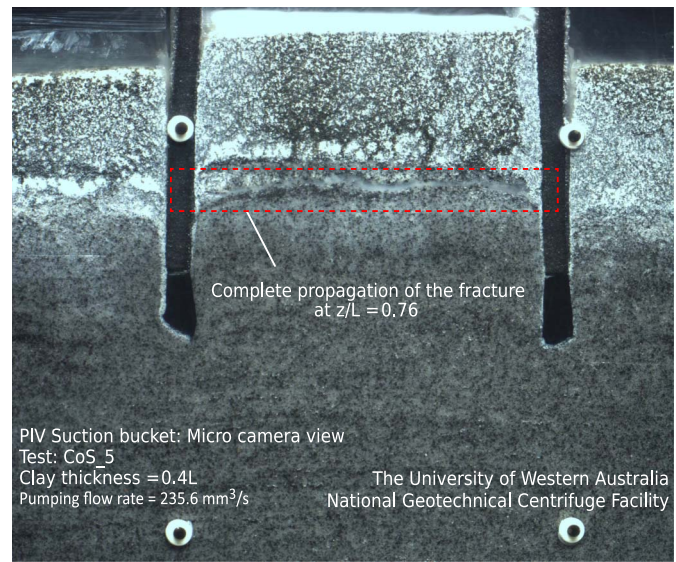


Fig. 21. Complete propagation of the fracture at the sand-clay interface in test CoS_5 (medium pumping flow rate) during suction-assisted installation at $z/L = 0.76$.

6, respectively) as the effect of the overlying clay layer on the response in the underlying sand was the focus of the investigation, and suction bucket installation in clay is well understood. The vertical load at $0.1 L$ in the sand layer was then held constant as V_{s-w} , which led to larger self-weight load with increasing h_{clay} (see V_{s-w} in Table 4 for CoS_3, 5, 6), but allowed for consistency of the self-weight embedment.

In both tests with increased clay thickness, the deformation mechanism while penetrating the clay layer was mainly localized around the skirt tips, and minor plug heave was observed at the end of the self-weight stage ($h_{plug}/L \sim 0.03$ at $z_{s-w}/L = 0.5$ for CoS_5, and $h_{plug}/L \sim 0.05$ at $z_{s-w}/L = 0.7$ for CoS_6).

A medium pumping flow rate, $q_{pump} = 235.62 \text{ mm}^3/\text{s}$, was used for the suction-assisted stage. Fig. 19 compares the resultant soil displacement contours for the three tests with increasing $h_{clay} = 0.2, 0.4, 0.6 L$ [CoS_3, 5, 6 in Figs. 19(a–c) respectively] at $z_{PIV}/L = 0.75$. A twofold increase in clay thickness [$h_{clay} = 0.4 L$, CoS_5, Fig. 19(b)] shows a response comparable to $h_{clay} = 0.2 L$ [CoS_3, $q_{pump} = 235.62 \text{ mm}^3/\text{s}$, Fig. 19(a)] during suction-assisted installation. Inverted V shear bands propagating from the skirt tips characterize the deformation mechanism, with prevalent inflow of material inside the bucket. A threefold increase in clay thickness [$h_{clay} = 0.6 L$, CoS_6, Fig. 19(c)] also resulted in the development of inverted V shear bands after the syringe pump was activated at $z_{s-w}/L = 0.7$. However, these were confined to the sand layer and did not expand to the clay above, such that the inverted V became less pronounced as the clay thickness increased (penetration in sand was limited to $0.6 < z/L < 1$).

The normalized penetration rate for CoS_5 ($h_{clay} = 0.4$) [Fig. 12(b)] is initially approximately constant (for $0.5 < z/L < 0.65$), but reduces from $z/L \sim 0.65$, at which point discolored fluid (i.e., fluid mixed with clay) appeared above the soil plug (Fig. 20). This is considered to be the result of seepage occurring along the skirts and/or through cracks in the clay [a possibility proposed by Senders et al. 2007]. The fracture at the clay-sand interface visible in Fig. 19(b) (and Fig. 21) fully propagated when $p/\gamma'_s D \sim 0.87$ at $z/L = 0.76$ (relative to the calculated value of $p_{plug}/\gamma'_s D = 0.54$ [Eq. (3)], i.e., underestimated by ~38%). When contact of the lid against the clay plug was achieved (Fig. 22) at $z_{fin}/L = 0.86$,

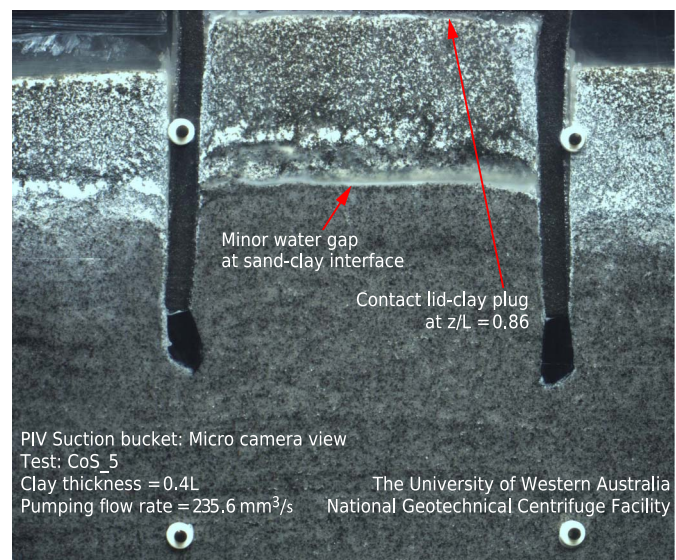


Fig. 22. Contact between clay plug and bucket lid at the end of suction-assisted installation in test CoS_5 (medium pumping flow rate) at $z/L = 0.86$.

a final plug heave $h_{plug}/L = 0.13$ was measured, which included a minor water gap ($<0.01 L$) at the clay-sand interface. As for $h_{clay} = 0.2 L$ (CoS_3), a reduction of the plug heave was observed when pumping was stopped and the clay plug came to rest on the underlying sand.

The constant normalized penetration rate for CoS_6 in Fig. 12(b) confirms the absence of any seepage flow through the thick clay layer ($h_{clay} = 0.6 L$) during suction-assisted installation. No clay plug uplift was observed, since the measured suction never reached the predicted $p_{plug}/\gamma'_s D = 0.86$ required for clay plug uplift. The final installation depth of $z_{fin}/L = 0.92$ (contact lid-surface) was larger than the tests with $h_{clay} = 0.4$ ($z_{fin}/L = 0.86$, CoS_5), and

$h_{\text{clay}} = 0.2$ ($z_{\text{fin}}/L = 0.8$, CoS_3). The final plug heave $h_{\text{plug}}/L = 0.09$ was the smallest across the three clay thicknesses investigated, due to (1) reduced suction-assisted installation; (2) negligible seepage flow through the sand, which limited volumetric expansion; and (3) minimal clay plug disturbance caused by suction.

Conclusions

The effects of a clay layer on suction bucket installation in dense sand were investigated through a visual study in a geotechnical centrifuge. PIV analyses conducted on images captured during suction bucket installations revealed the following:

1. Installations in sand-over-clay were relatively straightforward, as expected. Jacked and suction-assisted installations resulted in similar mechanisms overall, characterized by high shear strains along the skirts and limited volume change within the soil plug. Seepage flow was maintained when the skirt tips reached the clay layer, due to downward migration of the sand-clay interface. Further investigation should focus on establishing the response when the clay is more competent (i.e., stronger and stiffer);
2. Installations in clay-over-sand were also successful. The clay layer represented an effective blockage for seepage flow until clay plug uplift (detachment at the clay-sand interface) occurred. The results revealed that clay plug uplift allows suction to be transferred to the underlying sand layer. This has the effect of reducing the tip resistance through seepage flow, despite the overlying (relatively) impermeable layer, easing installation in the dense sand layer. The deformation mechanism was comparable to installations in sand only, although characterized by less volumetric expansion of the sand plug;
3. Clay plug uplift did not cause premature termination of suction bucket installation, although consideration should be given to the potential for clay ingress to compromise the efficiency of the pumping system. Uplift disturbed the clay plug upon completion of the installation process, with detachment evident at the clay-sand interface. The potential effect on the in-service performance of the suction bucket requires further investigation; and
4. Increasing pumping flow rates in clay-over-sand led to larger final penetration depths and faster installation, as well as a reduced clay plug uplift. Higher pumping flow rates may avoid refusal of suction buckets during installation in such profiles.

Data Availability Statement

The data obtained from the centrifuge tests are available from the corresponding author by request. GeoPIV-RG is a free image analysis module for MATLAB designed for geotechnical and structural engineering research applications, available from <http://www.geopivrg.com/>.

Acknowledgments

This work forms part of the activities of the Centre for Offshore Foundation Systems (COFS), which is currently supported as a Centre of Excellence by the Lloyd's Register Foundation. Lloyd's Register Foundation helps to protect life and property by supporting engineering-related education, public engagement and the application of research. This research is also supported through the Australian Research Council Linkage Project 180100024. The authors are grateful for this support. The views presented in this

paper represent those of the authors and not necessarily those of their respective employers.

References

- Andersen, K. H., H. P. Jostad, and R. Dyvik. 2008. "Penetration resistance of offshore skirted foundations and anchors in dense sand." *J. Geotech. Geoenviron. Eng.* 134 (1): 106–116. [https://doi.org/10.1061/\(ASCE\)1090-0241\(2008\)134:1\(106\)](https://doi.org/10.1061/(ASCE)1090-0241(2008)134:1(106)).
- Andersen, K. H., J. D. Murff, M. F. Randolph, E. C. Cluckey, C. T. Erbrich, H. P. Jostad, B. Hansen, C. Aubeny, P. Sharma, and C. Supachawarote. 2005. "Suction anchors for deepwater applications." In *Proc., Int. Symp. Frontiers in Offshore Geotechnics, ISFOG05*, 3–30. London: CRC Press.
- Bienien, B., R. T. Klinkvort, C. D. O'Loughlin, F. Zhu, and B. W. Byrne. 2018. "Suction caisson in dense sand, part I: Installation, limiting capacity and drainage." *Géotechnique* 68 (11): 937–952. <https://doi.org/10.1680/jgeot.16.P.281>.
- Chow, S. H., A. Roy, M. Herduin, E. Heins, L. King, B. Bienien, C. D. O'Loughlin, C. Gaudin, and M. J. Cassidy. 2019. *Characterisation of UWA superfine silica sand*, 33. GEO Rep. 18844. Crawley, Australia: Univ. of Western Australia.
- Cocjin, M. L., S. M. Gourvenec, D. J. White, and M. F. Randolph. 2014. "Tolerably mobile subsea foundations—Observations of performance." *Géotechnique* 64 (11): 895–909. <https://doi.org/10.1680/geot.14.P.098>.
- Cotter, O. 2009. "The installation of suction caisson foundations for offshore renewable energy structures." Ph.D. thesis, Dept. of Engineering Science, Univ. of Oxford.
- Cotterill, C. J., E. Phillips, L. James, C. F. Forsberg, T. I. Tjelta, G. Carter, and D. Dove. 2017. "The evolution of the Dogger Bank, North Sea: A complex history of terrestrial, glacial and marine environmental change." *Quat. Sci. Rev.* 171 (Sep): 136–153. <https://doi.org/10.1016/j.quascirev.2017.07.006>.
- Craig, W. H., and K. Chua. 1990. "Deep penetration of spudcan foundations on sand and clay." *Géotechnique* 40 (4): 541–556. <https://doi.org/10.1680/geot.1990.40.4.541>.
- Dewoolkar, M. M., H. Y. Ko, A. T. Stadler, and S. M. F. Astaneh. 1999. "A substitute pore fluid for seismic centrifuge modeling." *Geotech. Test. J.* 22 (3): 196–210. <https://doi.org/10.1520/GTJ11111J>.
- Dove, D., D. H. Roberts, D. J. A. Evans, D. R. Tappin, J. R. Lee, D. Long, C. L. Mellett, and S. L. Callard. 2016. "Refining glacial stratigraphy in the Southern North Sea—New bathymetric model brings renewed value to legacy seismic." In *Proc., Near Surface Geoscience 2016—Second Applied Shallow Marine Geophysics Conf.* Barcelona, Spain: European Association of Geoscientists and Engineers.
- DOW (Dow Chemical Company). 2002. *Methocel cellulose ethers*. Midland, MI: Technical Handbook Dow.
- Erbrich, C. T., and T. I. Tjelta. 1999. "Installation of bucket foundations and suction caissons in sand—Geotechnical performance." In *Proc., Offshore Technology Conf.* Richardson, TX: Offshore Technology Conference.
- Haigh, S. K., and S. P. G. Madabhushi. 2014. "Discussion of 'Performance of a transparent flexible shear beam container for geotechnical centrifuge modelling of dynamic problems' by Ghayoomi, Dashti and McCartney." *Soil Dyn. Earthquake Eng.* 67 (Dec): 359–362. <https://doi.org/10.1016/j.soildyn.2014.02.003>.
- Houlsby, G. T., and B. W. Byrne. 2005a. "Design procedures for installation of suction caissons in clay and other materials." *Proc. Inst. Civ. Eng. Geotech. Eng.* 158 (2): 75–82. <https://doi.org/10.1680/geng.2005.158.2.75>.
- Houlsby, G. T., and B. W. Byrne. 2005b. "Design procedures for installation of suction buckets in sand." *Proc. Inst. Civ. Eng. Geotech. Eng.* 158 (3): 135–144. <https://doi.org/10.1680/geng.2005.158.3.135>.
- Lacal-Arántegui, R., J. M. Yusta, and J. A. Domínguez-Navarro. 2018. "Offshore wind installation: Analysing the evidence behind improvements in installation time." *Renewable Sustainable Energy Rev.* 92 (Sep): 133–145. <https://doi.org/10.1016/j.rser.2018.04.044>.
- Ladd, C. C., R. Foot, K. Ishihara, F. Schlosser, and H. G. Poulos. 1977. "Stress-deformation and strength characteristics." In *Proc., Int. Conf.*

- Soil Mechanical Foundation Engineering*, 421–494. Tokyo: Japanese Society of Soil Mechanics and Foundation Engineering.
- Lee, K. K., M. F. Randolph, and M. J. Cassidy. 2013. "Bearing capacity on sand overlying clay soils: A simplified conceptual model." *Géotechnique* 63 (15): 1285–1297. <https://doi.org/10.1680/geot.12.P176>.
- Martin, C. M., and M. F. Randolph. 2006. "Upper-bound analysis of lateral pile capacity in cohesive soil." *Géotechnique* 56 (2): 141–145. <https://doi.org/10.1680/geot.2006.56.2.141>.
- Meyerhof, G. G. 1974. "Ultimate bearing capacity of footings on sand layer overlying clay." *Can. Geotech. J.* 11 (2): 223–229. <https://doi.org/10.1139/t74-018>.
- Morton, J. P., C. D. O'Loughlin, and D. J. White. 2014. "Strength assessment during shallow penetration of a sphere in clay." *Géotech. Lett.* 4 (4): 262–266. <https://doi.org/10.1680/geolett.14.00049>.
- O'Beirne, C., C. D. O'Loughlin, and C. Gaudin. 2015. "Soil response in the wake of dynamically installed projectiles." *Géotech. Lett.* 5 (3): 153–160. <https://doi.org/10.1680/jgele.15.00055>.
- Offshorewind.biz. 2018. "Last EOWDC turbine installed, inter-array cabling nearing completion". Accessed March 14, 2019. <https://www.offshorewind.biz/2018/05/28/last-eowdc-turbine-installed-inter-array-cabling-nearing-completion/>.
- Panayides, S., T. A. Powell, and K. Schröder. 2017. "Penetration resistance of suction caissons in layered soils—A case study." In *Proc., Int. Conf., Society for Underwater Technology, Offshore Site Investigation and Geotechnics (SUT-OSIG)*, 562–569. London: Royal Geographical Society.
- Qiu, G., and J. Grabe. 2012. "Numerical investigation of bearing capacity due to spudcan penetration in sand overlying clay." *Can. Geotech. J.* 49 (12): 1393–1407. <https://doi.org/10.1139/t2012-085>.
- Ragni, R., B. Bienen, S. A. Stanier, C. O'Loughlin, and M. J. Cassidy. 2019. "Observations during suction bucket installation in sand." *Int. J. Phys. Modell. Geotech.* <https://doi.org/10.1680/jphmg.18.00071>.
- Randolph, M. F., and C. Gaudin. 2017. "Genesis of the national geotechnical centrifuge facility—A 30 year perspective." *Aust. Geomech. J.* 52 (2): 1–14.
- Randolph, M. F., R. J. Jewell, K. J. L. Stone, and T. A. Brown. 1991. "Establishing a new centrifuge facility." In *Proc., Int. Conf. Centrifuge*, 3–9. Rotterdam, Netherlands: A.A. Balkema.
- Saue, M., P. M. Aas, K. H. Andersen, and E. Solhjell. 2017. "Installation of suction anchors in layered soils." In *Proc., Int. Conf., Society for Underwater Technology, Offshore Site Investigation and Geotechnics (SUT-OSIG)*, 507–515. London: Royal Geographical Society.
- Senders, M. 2008. "Suction caissons in sand as tripod foundations for offshore wind turbines." Ph.D. thesis, Centre for Offshore Foundation Systems, Univ. of Western Australia.
- Senders, M., and M. F. Randolph. 2009. "CPT-based method for the installation of suction buckets in sand." *J. Geotech. Geoenvir. Eng.* 135 (1): 14–25. [https://doi.org/10.1061/\(ASCE\)1090-0241\(2009\)135:1\(14\)](https://doi.org/10.1061/(ASCE)1090-0241(2009)135:1(14)).
- Senders, M., M. F. Randolph, and C. Gaudin. 2007. "Theory for the installation of suction caissons in sand overlaid by clay." In *Proc., Int. Conf., Society for Underwater Technology, Offshore Site Investigation and Geotechnics (SUT-OSIG)*, 429–438. London: Royal Geographical Society.
- Stanier, S. A., J. Blaber, W. A. Take, and D. J. White. 2016. "Improved image-based deformation measurement for geotechnical applications." *Can. Geotech. J.* 53 (5): 727–739. <https://doi.org/10.1139/cgj-2015-0253>.
- Stanier, S. A., and D. J. White. 2013. "Improved image-based deformation measurement in the centrifuge environment." *Geotech. Test. J.* 36 (6): 20130044. <https://doi.org/10.1520/GTJ20130044>.
- Stewart, D. P. 1992. "Lateral loading of piled bridge abutments due to embankment construction." Ph.D. thesis, Dept. of Civil Engineering, Univ. of Western Australia.
- Sturm H. 2017. "Design aspects of suction caissons for offshore wind turbine foundations." In *Proc., TC 209 Workshop-Int. Conf. on Soil Mechanics and Geotechnical Engineering*, 45–63. London: CRC Press.
- Tan, T. S., and R. F. Scott. 1985. "Centrifuge scaling considerations for fluid-particle systems." *Géotechnique* 35 (4): 461–470. <https://doi.org/10.1680/geot.1985.35.4.461>.
- Taylor, R. N. 1987. "Discussion of 'Centrifuge scaling considerations for fluid-particle systems' by Tan, T.S. and Scott, R.F. (1985)." *Géotechnique* 37 (1): 131–133.
- Teh, K. L., M. J. Cassidy, C. F. Leung, Y. K. Chow, M. F. Randolph, and C. K. Quah. 2008. "Revealing the bearing failure mechanisms of a penetrating spudcan through sand overlaying clay." *Géotechnique* 58 (10): 793–804. <https://doi.org/10.1680/geot.2008.58.10.793>.
- Teng, Y., S. A. Stanier, and S. M. Gourvenec. 2017. "Synchronised multi-scale image analysis of soil deformations." *Int. J. Phys. Modell. Geotech.* 17 (1): 53–71. <https://doi.org/10.1680/jphmg.15.00058>.
- Tran, M. N. 2005. "Installation of suction buckets in dense sand and the influence of silt and cemented layers." Ph.D. thesis, Centre for Offshore Foundation Systems, Univ. of Sydney.
- Tran, M. N., and M. F. Randolph. 2008. "Variation of suction pressure during caisson installation in sand." *Géotechnique* 58 (1): 1–11. <https://doi.org/10.1680/geot.2008.58.1.1>.
- Tran, M. N., M. F. Randolph, and D. W. Airey. 2007. "Installation of suction caissons in sand with silt layers." *J. Geotech. Geoenvir. Eng.* 133 (10): 1183–1191. [https://doi.org/10.1061/\(ASCE\)1090-0241\(2007\)133:10\(1183\)](https://doi.org/10.1061/(ASCE)1090-0241(2007)133:10(1183)).
- Watson, P. G., C. Gaudin, M. Senders, and M. F. Randolph. 2006. "Installation of suction caisson in layered soil." In *Proc., Int. Conf. on Physical Modelling in Geotechnics*, 685–692. London: CRC Press.
- Zhu, F. 2018. "Suction caisson foundations for offshore wind energy installations in layered soils." Ph.D. thesis, Centre for Offshore Foundation Systems, Univ. of Western Australia.